HBRC Journal (2016) **12**, 123–136

Housing and Building National Research Center

HBRC Journal

http://ees.elsevier.com/hbrcj

Modeling of shear deficient beams by the mixed smeared/discrete cracking approach

Dina Muhammad Fathi Ors [a,*], **Hussein Osama Okail** [b], **Amr Hussein Zaher** [b]

[a] *Structural Engineering and Construction Management Department, Future University in Egypt, Egypt*
[b] *Structural Engineering Department, Ain Shams University, Egypt*

Received 12 August 2014; revised 19 October 2014; accepted 2 November 2014

KEYWORDS

Beams;
Shear critical;
Smeared cracks;
Discrete cracks;
Stirrups

Abstract This paper presents an analytical study on the modeling of shear critical reinforced concrete beams modeled using the finite element method. The paper investigates two modeling strategies; the first of which is the well established smeared cracking modeling approach. Experimental test results from a wide range of beams tested by other researchers were used for model verification. This paper presents a mixed modeling approach in which the smeared cracking model was used in conjunction with discrete cracking planes to model the concrete continuums in an effort to reach a better correlation with the experimental data. This is achieved by introducing a specific plane inclined at angles in a specified range determined as a result of matching these models' behavior with behavior monitored in the experimental work at the suspected plane of failure for shear critical beams. Analytical results have shown that the proposed modeling approach is capable of better simulation of the observed experimental response in terms of strength and stiffness, as well as capturing the post-peak response of the tested beams. Errors have been calculated between analytical and experimental results; these errors are also acceptable within the bounds of the engineering judgment. Finally the mixed smeared/discrete cracking model is validated and can be used with a high degree of confidence to conduct further parametric studies.

Introduction

In the early 1900s, many methods were developed with the aim of investigating the most realistic load transfer method from loading plates to supports starting with Ritter (1899) who first used truss models as conceptual tools in the analysis and design of reinforced concrete beams.

Talbot (1909) confirmed this finding and pointed out the fallacies of such procedures as early as 1909 in talking about the failure of beams without web reinforcement. Based on 106 beam tests, it was concluded that the shear stress is greatly

* Corresponding author.
Peer review under responsibility of Housing and Building National Research Center.

Production and hosting by Elsevier

http://dx.doi.org/10.1016/j.hbrcj.2014.11.002

influenced by reinforcement ratio, beam span and other parameters which affect the stiffness of the beam. In beams without web reinforcement, beam shear resistance depends upon the quality and strength of the concrete. The stiffer the beam the larger the transverse stresses which may be developed. Short, deep beams give higher results than long slender ones, and beams with a high percentage of reinforcement give higher results than beams with a small reinforcement ratio.

Kani (1964) reported a more realistic approach in which the beam segments between the inclined flexural cracks act analogous to tooth in the comb thus behaving like a cantilever. Collins and Mitchell (1974) based on the Wagner theory developed a method for determining the inclination of the principal stress "θ" applicable over the full loading range for members subjected to torsion. This procedure is called the "compression field theory (CFT)". Later, Vecchio and Collins (1986) presented the Modified Compression Field Theory (MCFT) extending the first theory to members subjected to shear.

The MCFT is a further enhancement of the CFT that accounts for the influence of the tensile stresses in cracked concrete that was ignored in truss models. Belarbi and Hsu (1994, 1995) developed a procedure called the Rotating Angle Softened Truss Model (RA-STM) to account for tensile stresses in diagonally cracked concrete. Like MCFT, this method assumes that the inclination of the principal stress, θ, coincides with the principal strain direction. Vecchio 2001, held an analytical investigation using finite element analysis (FEA) as an extension of MCFT; the hybrid crack shear slip formulation is found to accurately model the divergence of stress and strain directions, providing an improved representation of behavior. He also found that predictions of shear strength and failure mode are significantly influenced in some cases. Sahibzada Farooq et al. (2013), developed the compressive force path (CFP) method to explain shear behavior of reinforced concrete (RC) beams identifying types of beams according to its shear span-to-depth ratio.

From all previous researches, it became clear that one of the major disadvantages of shear critical reinforced concrete elements is that failure occurs due to one single crack with approximately no significant damage in the rest of the reinforced concrete element [1], which makes it difficult to develop a model with the whole element stiffness to resist a failure due to this single crack without predicting at least an approximate failure surface with the aim of getting close to the realistic ductile behavior of the element monitored through previous experimental works. This study will investigate a different approach in modeling shear critical reinforced concrete elements.

Reference experimental investigation

Deep beams with variable web reinforcement [2]

Test specimen description

Test specimens consisted of sixteen simply supported concrete deep beams with different properties tested by *A. Arabzadeh, R. Aghayari and A. Rahai* in 2011[2]. They were classified into four series according to the type of their web reinforcing. All specimens had a rectangular cross-section with 80 mm × 400 mm. Their overall and effective spans were 1600 mm and 1200 mm, respectively. Fig. 1 and Table 1 give additional details of the specimens.

Phase one: Series **A** consists of six deep beams with variable transverse steel bars and uniform spacing.

Phase two: Series **B** consists of three deep beams with variable transverse steel bars concentrated at the center of shear span.

Phase three: Series **C** consists of four deep beams reinforced by variable longitudinal and constant transverse web reinforcements.

Phase four: Series **D** consists of three deep beams reinforced by diagonal steel bars which are placed perpendicular to the expected diagonal cracks.

Materials

Concrete. The concrete was prepared by Type II Portland cement and river fine aggregate. Maximum aggregate size was 12.5 mm and the slump was approximately 90 mm. The concrete strength was defined based on the average value of three standard cylinders (300 × 150 mm).

Reinforcing steel. The longitudinal steel reinforcement consisted of 12D (12 mm diameter), 22D (22 mm diameter) and 25D (25 mm diameter) deformed steel bars, and also steel shear reinforcement included 6D (6 mm diameter) smooth round bars. Mechanical properties of used steel bars are indicated in Table 4.

Beam specimens with variable web reinforcement ratio and shear span-to-depth ratio [3]

Test specimen description

Ten deep beams under four point bending were constructed and loaded to failure by *J. Dedios, A. Lubell* in 2008 [3]. These beams were designed considering variation of longitudinal reinforcement ratio, shear span-to-depth ratio and presence/omission of transverse web reinforcement. The strength of longitudinal reinforcement was studied through comparison against specimens with normal strength reinforcement. Other parameters shown to influence the performance of non-slender beams, such as concrete strength, transverse web reinforcement distribution, spacing between bars and reinforcement development lengths were designed as constant.

Longitudinal Reinforcement Type: (**M**): for high strength ASTM A1035 reinforcing steel and (**N**) for grade 400R reinforcing steel.

Transverse Reinforcement: (**S**): for specimens with web reinforcement and (**W**) for specimens without web reinforcement.

Shear Span-to-Depth Ratio: (**1**): for a/d = 1.19, (**2**) for a/b a/d = 1.78 and (**3**) for $a/d = 2.38$.

Percentage of Longitudinal Reinforcement: (**1**) for 1.15%, (**2**) for 1.13%, (**3**) for 2.29% and (**4**) for 1.77%.

The experimental program was divided into two test phases as follows.

Phase one specimens. Six beams were reinforced longitudinally with high strength steel and contained normal strength transverse web reinforcement and two specimens were built with main longitudinal and transverse reinforced normal strength steel reinforcement. These eight beams were further divided

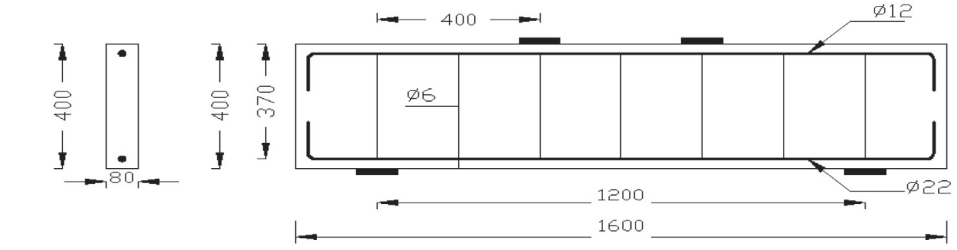

(a) The specimens' typical schema (All Dimensions are in Millimeters)

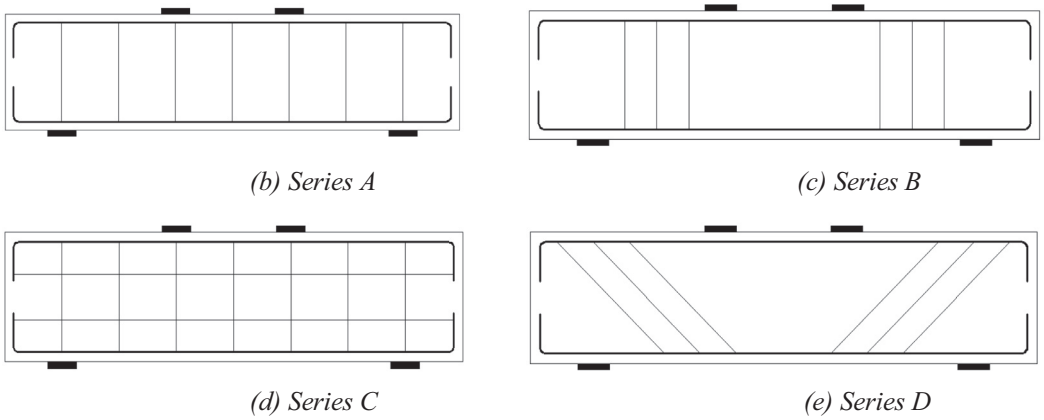

(b) Series A *(c) Series B*

(d) Series C *(e) Series D*

Fig. 1 Variations of web reinforcement in deep beams (A. Arabzadeh, R. Aghayari and A. Rahai, 2011) [2].

Table 1 Details of the tested beams (A. Arabzadeh1, R. Aghayari and A. Rahai, 2011) [2].

Series	ID	$f_{c'}$ MPa	Web reinforcement					
			Transverse		Longitudinal		Inclined	
			No.	ρ_v	No.	ρ_h	No.	ρ_i
A	A-1	59	–	–	–	–	–	–
	A-2	60	6–6D*	0.18	–	–	–	–
	A-3	61	10–6D	0.29	–	–	–	–
	A-4	60	16–6D	0.47	–	–	–	–
	A-5	65	21–6D	0.62	–	–	–	–
	A-6	60	28–6D	0.82	–	–	–	–
B	B-1	62.5	6–6D	0.18	–	–	–	–
	B-2	59	10–6D	0.29	–	–	–	–
	B-3	58	16–6D	0.47	–	–	–	–
C	C-1	58	10–6D	0.29	1–6D	0.10	–	–
	C-2	60	10–6D	0.29	2–6D	0.20	–	–
	C-3	60	10–6D	0.29	3–6D	0.30	–	–
	C-4	58	10–6D	0.29	4–6D	0.40	–	–
D	D-1	61	–	–	–	–	6–6D	0.42
	D-2	60	–	–	–	–	10–6D	0.70
	D-3	60	–	–	–	–	16–6D	1.00

* 6–6D: 6 transverse bars, 6 mm in diameter.

to five series according to their reinforcement ratio, shear span-to-depth and type of main reinforcing steel.

Phase two specimens. Two specimens were built with only longitudinal high strength steel and no web reinforcement. Details of the geometry and reinforcement configurations are summarized in Fig. 2, Tables 2 and 3.

Materials

Concrete. Initial design of the specimens was completed on the basis of normal strength concrete with a nominal compressive strength of 30 MPa. All concrete was supplied by a local ready-mix concrete company. Cylinder samples were made using molds 150 mm in diameter by 300 mm in height and were prepared by a certified technician in the day of casting. The

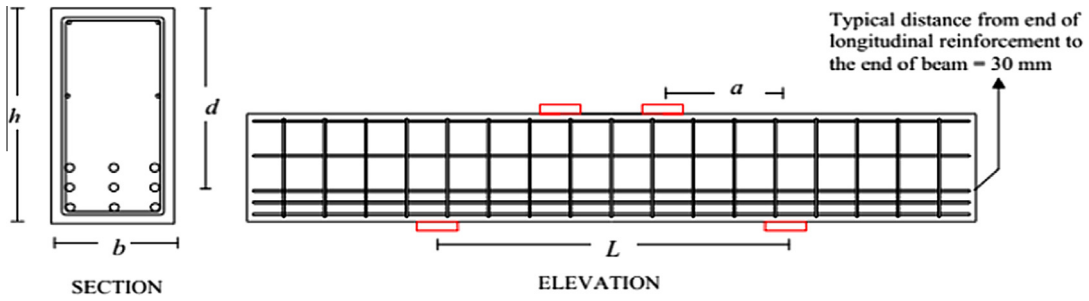

Fig. 2 Typical reinforcement details for beam specimens with variable web reinforcement ratio and shear span-to-depth ratio (J. Dedios, A. Lubell in 2008) [3].

Table 2 Mechanical properties of the steel bars.

Bar ID	Area (mm^2)	Yield strength (MPa)	Yield strain (mm/mm)	Ultimate strength (MPa)	Ultimate strain (mm/mm)	Young's modulus (MPa)
25D	491	557	0.0027	577	0.271	214,000
22D	380	585	0.0028	589	0.263	206,000
12D	113	433	0.0021	491	0.200	208,000
6D	28	397	0.0020	469	0.097	201,000

Table 3 Dimensions of tested beams (J. Dedios, A. Lubell in 2008) [3].

Phase	Series	Specimen ID	b (mm)	D (mm)	h (mm)	l (mm)	L (mm)	a (mm)	a/d –
1	1	MS1–1	300	501	607	1700	3560	600	1.19
	2	MS1–2	300	503	607	1700	3560	600	1.19
		MS2–2	300	503	607	2300	2300	900	1.79
		MS3–2	300	503	607	2900	2900	1200	2.38
	3	MS1–3	300	506	607	1700	3560	600	1.18
		MS2–3	300	506	607	2300	2300	900	1.78
	4	NS1–4	300	507	607	1700	3560	600	1.18
		NS2–4	300	507	607	2300	2300	900	1.80
2	1	MW1–2	300	503	607	1700	3560	600	1.19
		MW3–2	300	503	607	2900	2900	1200	2.38

Table 4 Test specimens' reinforcement details (J. Dedios, A. Lubell in 2008) [3].

Phase	Series	Specimen ID	Upper RFT	Lower RFT	Shrinkage bars	Transverse web reinforcement (Grade 400)	ρ_s (%)
1	1	MS1–1	2#4	6#4	2#3	10M@200mm	0.52
	2	MS1–2	2#4	6#6	2#4	10M@200mm	1.13
		MS2–2	2#4	6#6	2#4	10M@200mm	
		MS3–2	2#4	6#6	2#4	10M@150mm	
	3	MS1–3	2#4	9#7	2#3	10M@200mm	2.29
		MS2–3	2#4	9#7	2#4	10M@150mm	
	4	NS1–4	2–10M	9–20M	2–10M	10M@200mm	1.77
		NS2–4	2#4	9–20M	2#4	10M@200mm	1.77
2	1	MW1–2	2#4	6#6	N/A	N/A	1.13
		MW3–2	2#4	6#6	N/A	N/A	1.13

concrete strength obtained from the concrete supplier varied from 39 to 48 MPa for beams reinforcing with high strength steel. The concrete strength of 23 and 25 MPa was obtained for beams reinforcing with normal strength steel. The measured concrete strength values were used in the analysis of all specimens. The concrete strengths are listed in Table 5.

Reinforcing steel. The reinforcing steel used in this experimental work consisted of two different types of steel; Grade 400R reinforcing steel and ASTM A1035 reinforcing steel. 10 M and 20 M (Canadian standard sizes) Grade 400R reinforcing steel bars and #3, #4, #6, #7 (American standard sizes) ASTM A1035 reinforcing steel bars were used. See Table 6 for rebar properties.

Table 5 Test specimens' details (J. dedios, A. Lubell, 2008) [3].

Phase	Series	Specimen ID	Main RFT type	f_c' (MPa)
1	1	MS1–1	ASTM A1035	46
	2	MS1–2	ASTM A1035	44
		MS2–2	ASTM A1035	47
		MS3–2	ASTM A1035	48
	3	MS1–3	ASTM A1035	44
		MS2–3	ASTM A1035	43
	4	NS1–4	Grade 400R	23
		NS2–4	ASTM A1035	25
2	1	MW1–2	ASTM A1035	39
		MW3–2	ASTM A1035	43

Modeling strategy

The modeling approach used in this paper differs from the conventional modeling approach in the way the concrete beam is considered. Since the failure of the beam in shear occurs due to major diagonal cracks, the concrete continuum is modeled as a number of jointed solid polygons outlining the expected shear failure planes. Fig. 3 shows the typical beam failure in shear while Fig. 4 shows the development basis of the proposed scheme.

Through many trials of geometry with the aim of achieving proper failure to be compatible with the observed failure mechanism, the following input concrete parts have been chosen. Inclination angles used in these models were θ = (60°–70°) and Φ = (30°–60°).

The finite element software package ABAQUS-CAE version 6.10 was used in the nonlinear analyses of the beams. All beams simulated with the smeared model were also simulated by the proposed approach modeling technique in this paper for the sake of comparison.

Concrete model

There are several types of brick elements available in the ABAQUS. For the analysis attached, (C3D8) elements have been chosen with an approximate maximum mesh size of (10–15) % beam height to achieve a good level of accuracy of results. The mesh intensity is the same for the whole concrete part of every single model.

Reinforcement steel model

Discrete reinforcement bars can be defined only by three-dimensional truss elements with linear shape functions (T3D2). The elements were used with the same approximate maximum size used in beam parts for all reinforcement types.

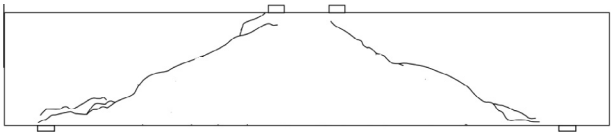

Fig. 3 Simple beam failure in shear.

Loading and supporting plates' model

Supporting and loading plates that transfer the reactions from and to the concrete elements are modeled as discrete rigid solid parts. Similar to concrete beam, the three dimensional solid element (C3D8) was chosen to model the steel plates in both loading and supporting positions with approximate maximum mesh size that is similar to that used for the concrete and reinforcing steel bars. Fig. 5 shows the used mesh and the different components of the modeled beams.

Material model

Concrete

Elastic behavior

The elastic behavior was modeled as linear and isotropic, standard values of modulus of elasticity of each concrete according to its grade and according to Euro code of Practice (table 3.1) are used. Its value can be calculated using the relation presented in Eq. (1).

$$E_{cm} = 22(0.1\, f_{cm})^{0.30} \tag{1}$$

To completely define the elastic behavior; Poisson's ratio should be defined. Concrete Poisson's ratio is determined from many previous works by testing several concretes and measured in the range of 0.15–0.20. In this study a value of 0.20 for Poisson's ratio was chosen.

Plasticity parameters in triaxial loading state

In order to describe strength with the equation for triaxial stress as input to the finite element program ABAQUS, a set of five parameters are required to completely describe the plastic behavior of concrete; $\mathbf{K_c}$, ϵ, $\boldsymbol{\sigma_{b0}/\sigma_{c0}}$, and $\boldsymbol{\psi}$, the default values are preferred to be used by the ABAQUS and its values are 2/3, 0.10, 1.16, and 36° respectively [4].

Table 6 Reinforcing steel properties (J. dedios, A. Lubell, 2008) [3].

Bar type	Area (mm2)	Yield strength (MPa)	Yield strain –	Ultimate strength (MPa)	Ultimate strain –	Young's modulus (MPa)
#3	71	855	0.0063	1067	0.047	197,250
#4	129	838	0.0063	1017	0.051	195,150
#6	284	870	0.0063	1040	0.039	203,300
#7	387	880	0.0065	1070	0.037	199,450
10 M	100	408	0.0021	660	0.083	204,850
20 M	300	401	0.0020	540	0.116	197,850

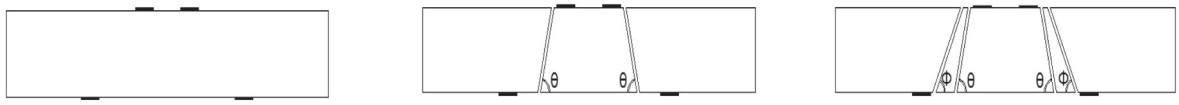

(a) Geometry of smeared cracking model *(b) Mixed smeared/cracking model* *(c) Refined mixed smeared/cracking model*

Fig. 4 Geometry of concrete model part(s) input to the ABAQUS and inclination angles varied in all specimens.

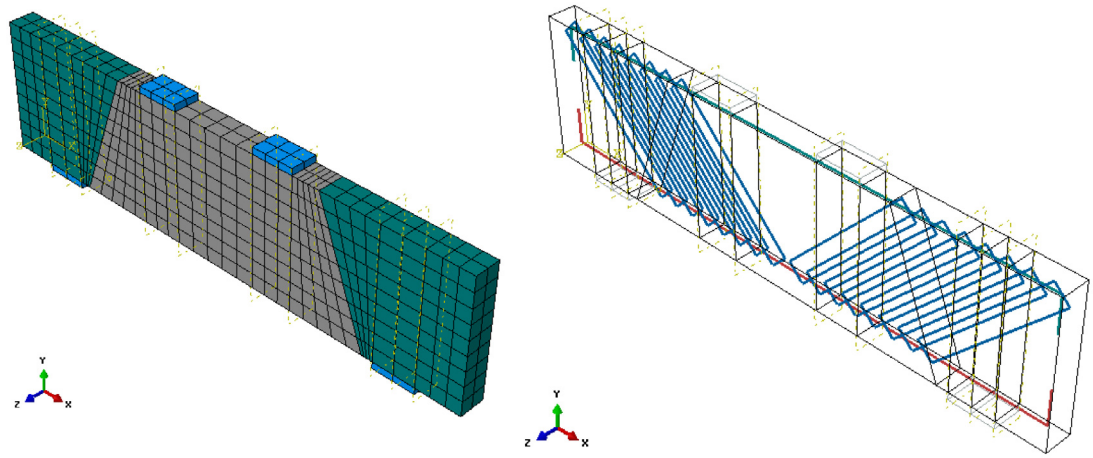

(a) *(b)*

Fig. 5 (a) 3D Meshing of Beam Parts and Supporting Plates. (b) Embedded RFT in the Beam Parts. (3D Views).

K_c: The ratio of the second stress invariant on the tensile meridian to that on the compressive meridian at initial yield for any given value of the pressure invariant P such that the maximum principle stress is negative, $\sigma_{max} < 0$. The default value is 2/3 [4].

Є: Plastic potential eccentricity. It is a small positive value which expresses the rate of approach of the plastic potential hyperbola to its asymptote. It can be calculated as a ratio of tensile strength to compressive strength. The CDP model recommends to assume ε = 0.1 [4].

σ_{b0}/σ_{c0}: The ratio of the strength in the biaxial state to the strength in the uniaxial state. The most reliable in this regard are the experimental results reported by Kupffer (1969). After their approximation with the elliptic equation [4], uniform biaxial compression strength f_{cc} is equal to 1.16248 f_{c0}. The ABAQUS user's manual specifies default $\boldsymbol{\sigma_{b0}/\sigma_{c0}} = 1.16$ [4].

ψ: Dilation angle. The angle of inclination of the failure surface toward the hydrostatic axis, measured in the meridional plane. Physically, dilation angle ψ is interpreted as a concrete internal friction angle. In simulations usually $\psi = 36°$ 0, 0 or $\psi = 40°$ 0 is assumed [4].

Compressive behavior

Concrete compressive behavior is input to the ABAQUS by applying the standard equation in Euro code (EN 1992-1-1) shown in Eq. (2).

$$\sigma_c = f_{cm} \cdot \frac{k\eta - \eta^2}{1 + (k-2)\eta} \tag{2}$$

where

$\eta = \varepsilon_c/\varepsilon_{c1}$

and $\varepsilon_{c1} = 0.7(f_{cm})^{0.31}\varepsilon_{cI}$ strain at peak stress according to (Euro code, Part1-1, 2004).

$k = 1.05E_{cm}.|\varepsilon_{c1}|/\mathbf{f_{cm}}$

Tensile behavior

Since tension stiffening may considerably affect the results of the analysis and the relation needs calibrating for a given simulation, it is proposed to use the modified Wang & Hsu formula for the weakening function as in Eq. (3).

$$\sigma_t = f_{ctm}\left(\frac{\varepsilon_{cr}}{\varepsilon_t}\right)^n \textit{if } \varepsilon_t > \varepsilon_{cr} \tag{3}$$

where σ_t is tensile stress at any point after peak, $\mathbf{f_{ctm}}$ is the tensile strength of concrete under uniaxial stress, power n is the rate of weakening, ε_{cr} is the strain at concrete cracking and ε_t is the strain at any point after peak.

Steel reinforcement model

The complete stress–strain relation is idealized and defined as the ABAQUS for all steel grades and the type by Mast el al. (2007) was used, see Eqs. (4) and (5).

$$\mathbf{f_s} = \mathbf{E_s}\boldsymbol{\varepsilon_s}\ (\mathbf{MPa})\ \varepsilon_s \leqslant \varepsilon_y \tag{4}$$

$$\mathbf{f_s = f_y\ (MPa)}\ \varepsilon_s \geqslant \varepsilon_y \tag{5}$$

The steel input data for all beams are taken as follows; in elastic zone; the elastic behavior was modeled as linear and isotropic and it is accepted and considered. The Modulus of elasticity (E_c) and Poisson's ratio (ν) of reinforcing steel are input to the ABAQUS for plastic behavior simulation. Plastic behavior is defined by parameters of stress and plastic strain at the onset of yielding (f_y, ε_y) and the stress and strain at ultimate (f_y, ε_u). Plastic strain can be calculated as shown in Eq. (6). These parameters can be derived from experimentally obtained stress–strain relations or from standard tables of reinforcing steel according to its grade if experimental data are not available.

$$\varepsilon_{pl} = \varepsilon_s - \varepsilon_y \tag{6}$$

Steel plate model

The steel plates were modeled using an isotropic linear elastic material model by Eq. (4) with solid elements for all models. The assumption for the material of loading and supporting plates is to avoid problems in solution due to the large deformations that will be developed or stress singularity in the plates.

Interactions

Concrete beam and steel reinforcement interaction

In this study, truss elements are used to represent the reinforcement, and these are embedded in "host" continuum solid elements as shown in Fig. 1. Embedding means that the translational degrees of freedom at the nodes of the embedded element are eliminated and become constrained to the corresponding interpolated values in the host continuum element.

Concrete beam and steel plate interaction

To avoid stress concentrations and singularities within the concrete beam, the reaction forces are transferred to the beam through plates defined as discrete rigid bodies. Plates transferring reactions from the supports are connected to the beam specimen using the "tie" option, which means that parts cannot be disconnected during loading.

Discrete cracking plane

Interaction behavior at predicted failure surfaces at localized compressive failure zone is the main controlling aspect of this modeling strategy. The following subsection describes the formulations of such failure surface.

Cohesive behavior. Cohesive behavior has been defined with the aim of introducing the natural contact between the two surfaces in the intact concrete, also to have capability to define damage behavior of material at the interaction surface which is concrete in this case. Also through choosing this behavior; there is an option of allowing cohesive behavior during repeated post-failure contacts.

Damage behavior. In order to allow cohesion between the two surfaces to fail and separate due to shear failure, a damage

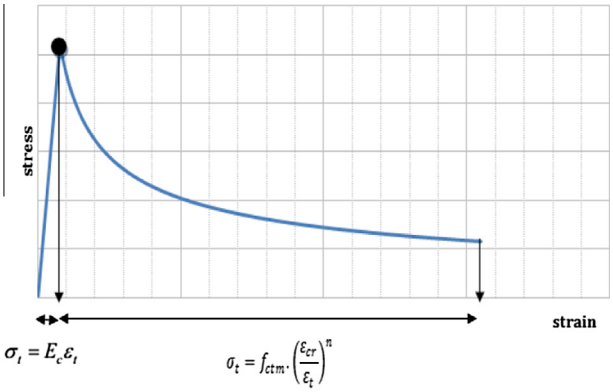

Fig. 6 Tensile damage definition at contact surfaces.

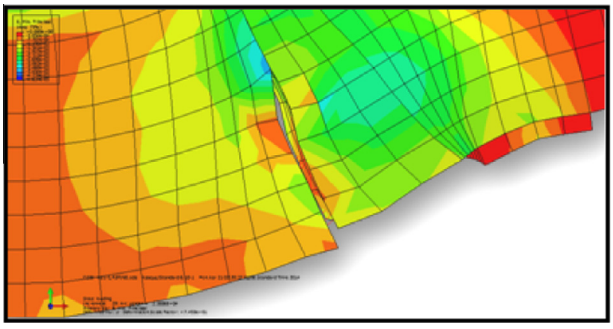

Fig. 7 Failure at predicted discrete cracking surfaces.

behavior should be defined according to material properties at this contact. As long as the main failure reason of all tested beam specimens in this study is the shear failure, diagonal tension stresses in the direction of principle tension stresses, are simulated as the failure surfaces, of concern to be chosen as failure surfaces as discussed in previous parts. The model of concrete in tension is used to define damage at contact surfaces as shown in Fig. 6.

Same interaction properties are defined for all shear critical reinforced concrete beam specimens in this study taking variations in concrete properties into consideration; namely, concrete strength in tension, modulus of elasticity, yield strain, ultimate strain concrete can achieve in tension and rate of weakening of concrete. As an implementation of (Vecchio 2001) who gave a particular attention to including crack shear slip in the description of element distortion and maximum strains, compatibility between his approaches and the proposed modeling approach represented in this study is matching to a great extent. Fig. 7 shows clearly the slippage and strains at the predicted surfaces in failure mode results from the application of the proposed approach modeling technique [5–7].

Results and analytical investigation

The investigation of shear critical reinforced concrete beams and their behavior using the mixed modeling approach as well as the smeared cracking model as a shear critical reinforced concrete elements is a subject of considerable interest in reinforced concrete structures, according to shear span-to-depth ratio and

web reinforcement the ultimate strength is generally controlled by shear rather than flexure, if sufficient amount of longitudinal reinforcement is used. In this section a comparison between results from experimental, smeared cracking, mixed smeared/discrete cracking model and the refined model is presented.

Failure modes

Beams with variable web reinforcement

The mixed smeared/discrete cracking model shows a realistic failure mode for all specimens for beams failing in shear. The smeared cracking model as well as the new approach shows the same response up to failure. In the early steps of loading, few transverse flexural cracks are formed in the pure-bending region. As the load increased approximately to 30–50% of the ultimate load, generally the diagonal cracks appeared at the mid-height of beam within the clear shear span in the direction of the main strut and propagated rapidly toward the outside edge of the loaded point and the inside edge of the support. Here the new modeling approach starts to give low load values while the diagonal cracks were developing and propagating in the center of shear span. Failure for most specimens was brittle shear failure and their failure mechanisms are identified as shown in Table 7.

Table 7 Comparison between the failure mechanisms of experimental, smeared cracked model mixed smeared/discrete cracking model for beams with variable web reinforcement.

Specimen ID	Experimental Failure Mechanism	Smeared Cracking Model Failure Mechanism	Mixed Smeared/Discrete cracking Model Failure Mechanism
A-1	N/A		
A-2	N/A		
A-3	N/A		
A-4			
A-5			
A-6			
B-1	N/A		
B-2	N/A		
B-3	N/A		
C-1	N/A		
C-2	N/A		
C-3	N/A		
C-4	N/A		
D-1	N/A		
D-2	N/A		
D-3			

Beams with transverse web reinforcement

The proposed modeling approach results prove the effectiveness of this modeling approach, as the ductility demand is closely matched and post peak behavior is improved to better match the experimental results obtained from the experimental work from previous researches presented earlier. Table 8 shows that refinement of this model improved the results and achieved more accuracy and matched to a great extent with the experimental results.

Table 8 Comparison between the failure mechanisms of experimental, smeared cracked model mixed smeared/discrete cracking model and refined mixed smeared/discrete cracking model for beams with transverse web reinforcement.

Specimen ID	Experimental Failure Mechanism Smeared Cracking Model Failure Mechanism	Mixed Smeared/Discrete Cracking Model Failure Mechanism Refined Mixed Smeared/Discrete Cracking Model Failure Mechanism
MS1-1	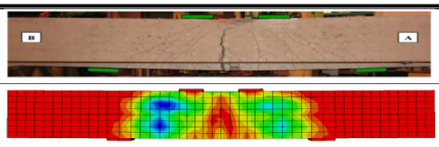	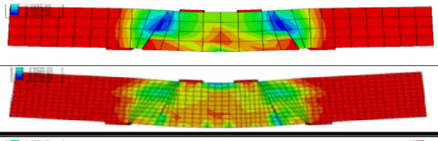
MS1-2	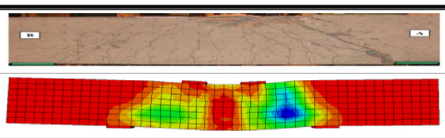	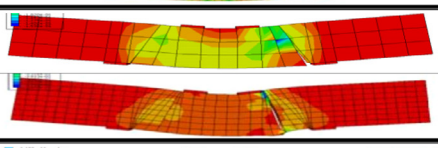
MS2-2	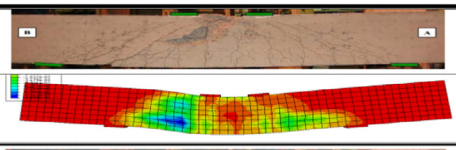	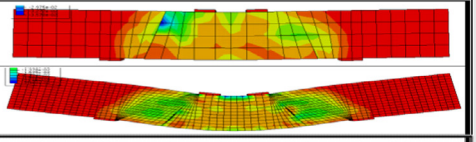
MS3-2	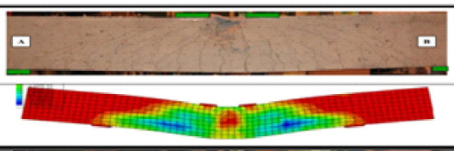	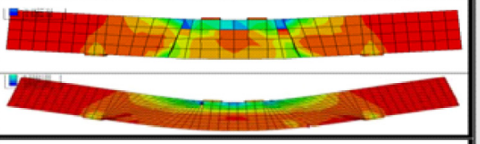
MS1-3	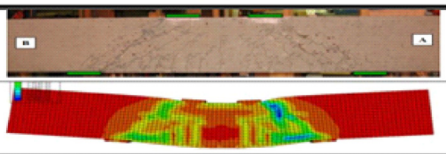	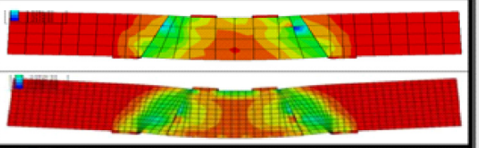
MS2-3	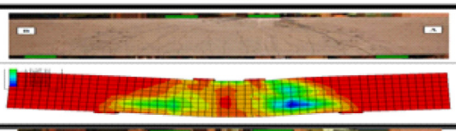	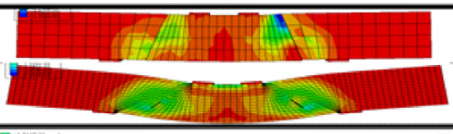
NS1-4	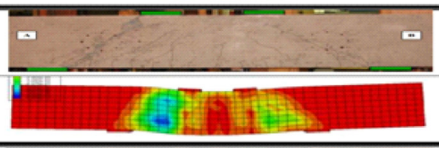	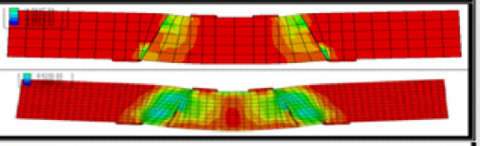
NS2-4	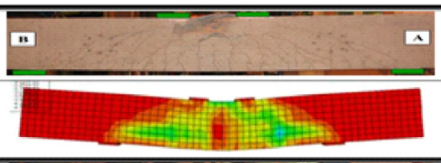	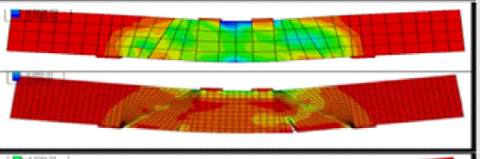
MW1-2	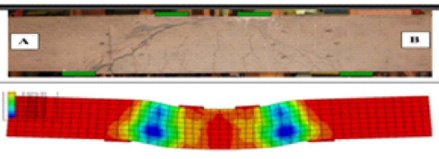	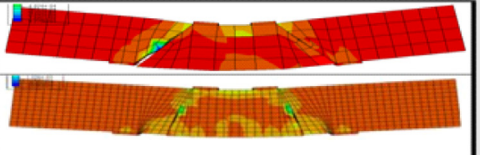
MW3-2	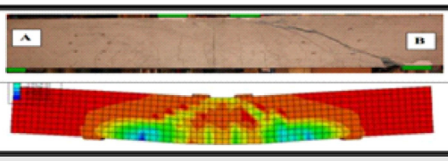	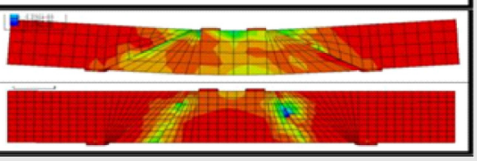

Load versus mid-span deflection curves

Beams with variable web reinforcement

Fig. 8 compares the load versus mid-span deflection curves for specimens of series A, B, C and D between the experimental, analytical model with the smeared cracking model and mixed smeared/discrete approach. The comparison shows a good match between all curves in terms of stiffness changes and the preserved trends in the pre- and post-cracking responses. The traditional model shows in most cases a more brittle

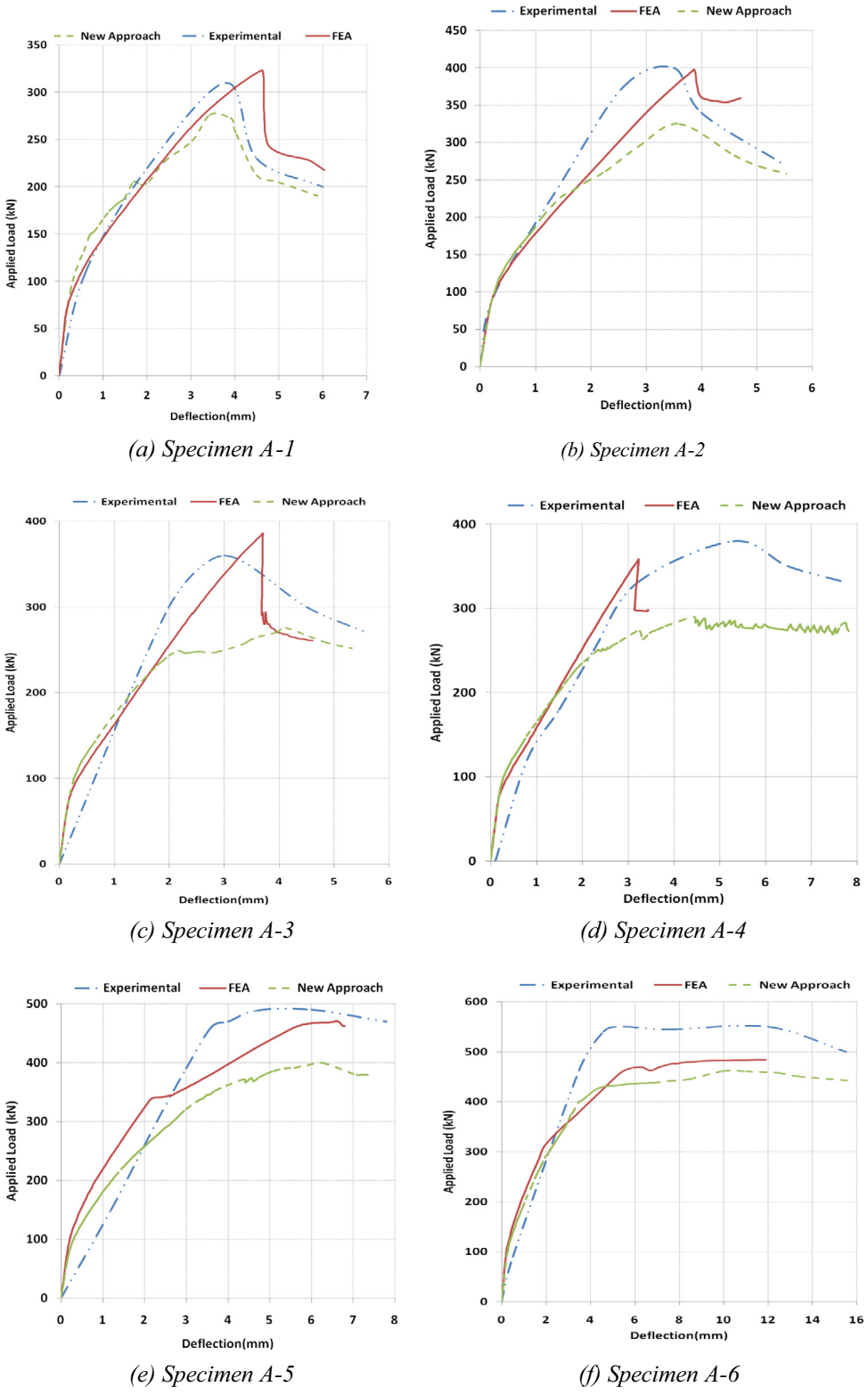

Fig. 8 Load versus mid-span deflection for beams with variable web reinforcement specimens.

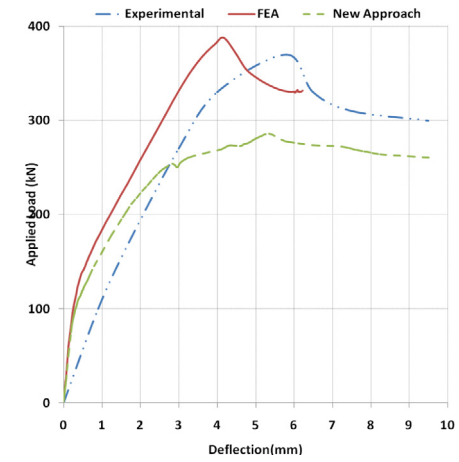

(g) Specimen B-1

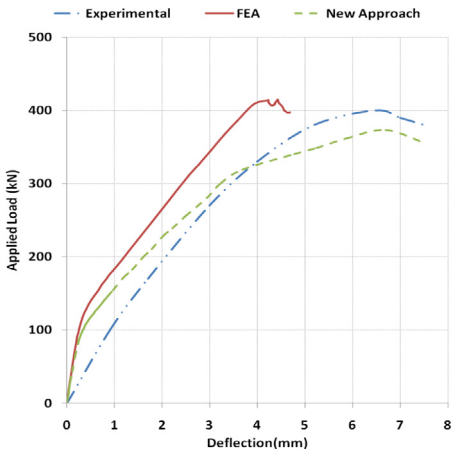

(h) Specimen B-2

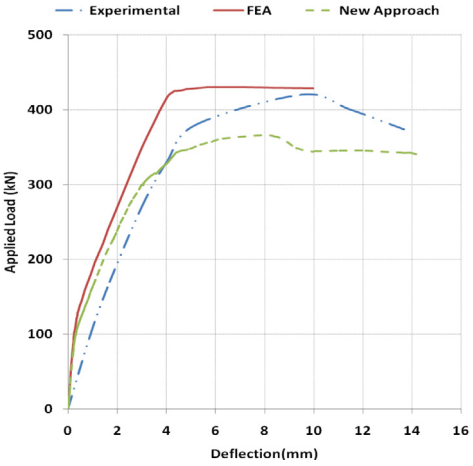

(i) Specimen B-3

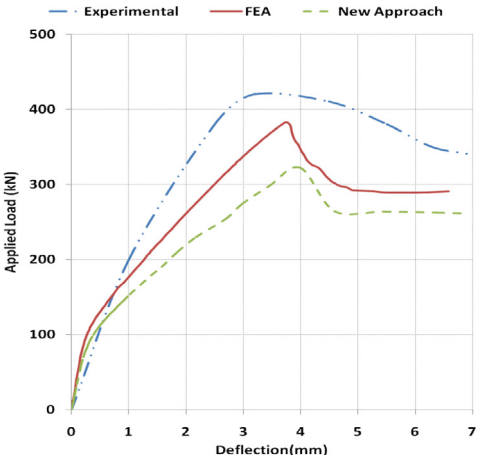

(j) Specimen C-1

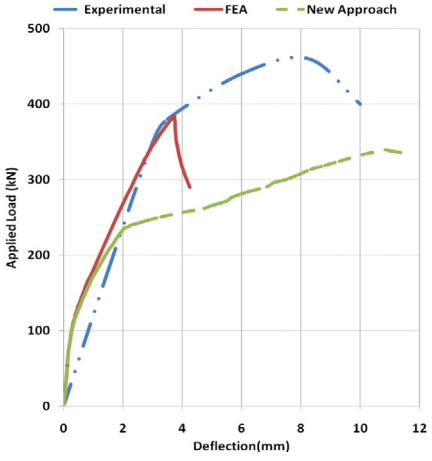

(k) Specimen C-2

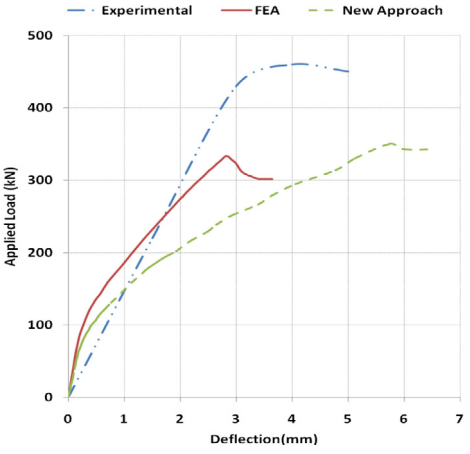

(l) Specimen C-3

Fig. 8 *(continued)*

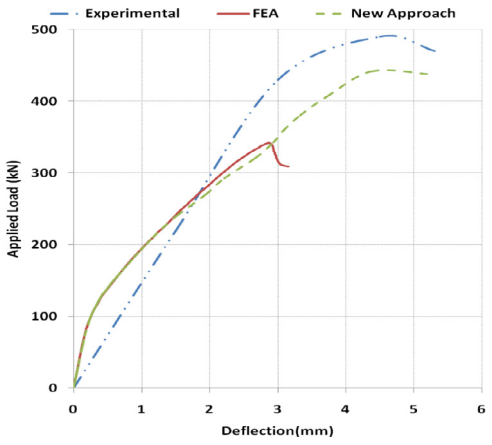

(m) Specimen C-4

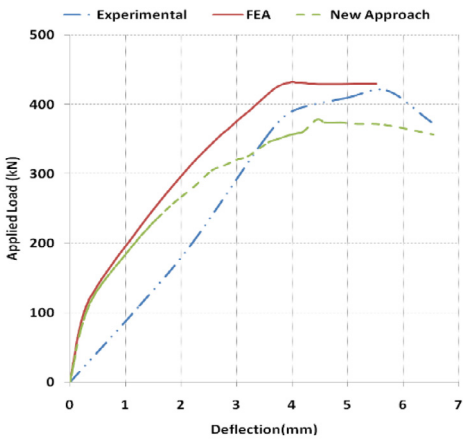

(n) Specimen D-1

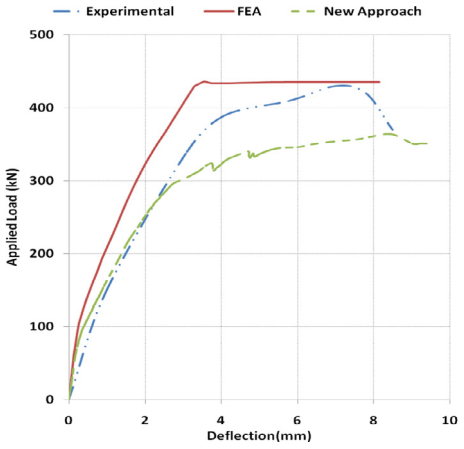

(o) Specimen D-2

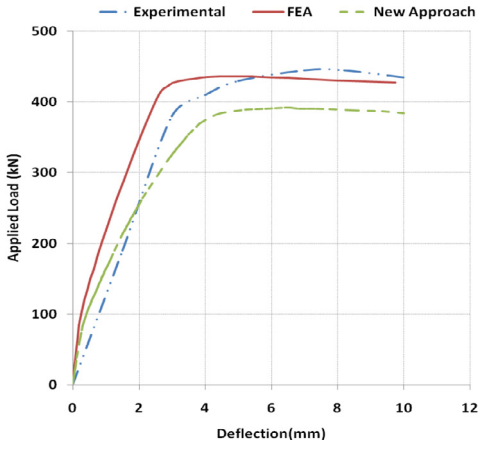

(p) Specimen D-3

Fig. 8 *(continued)*

failure; a problem which does not exist in the mixed approach model, as both models show that all specimens present a nearly linear behavior up to failure which was well represented by both modeling techniques, a rapid decrease in the initial stiffness at the appearance of major diagonal cracks which was better represented in the case of the new approach technique than the smeared one which always gives a low maximum strain value. Also in all three cases; applied load decreased suddenly once it attained the peak point due to the increasing shear distortions. In addition beyond the formation of major diagonal cracking, the beams with bigger shear reinforcement ratio behave stiffer than those reinforced with low web reinforcement. This means, before the formation of the diagonal cracks, shear reinforcement has no considerable effect on beam stiffness, but beyond the formation of major diagonal cracks it appears to have an enhancing effect on beam stiffness. Furthermore, the proposed approach in contrary to the purely smeared model was capable of displaying this ductile behavior accurately in most cases.

Beam specimens with variable web reinforcement ratio and shear span-to-depth ratio

Fig. 9 shows similar results from beams with variable web reinforcement ratio and shear span-to-depth ratio. The same conclusion may be drawn as before where the proposed mixed approach shows better potential in capturing the response of shear critical beams.

Model validation

From all these comparisons that were held in the previous sections between experimental and analytical models of smeared and mixed smeared/discrete approach models; good correlations were found between the numerical predictions and experimental results for the elastic stiffness, maximum load and the corresponding displacement, plateau displacement and failure mode of the specimens in all beams.

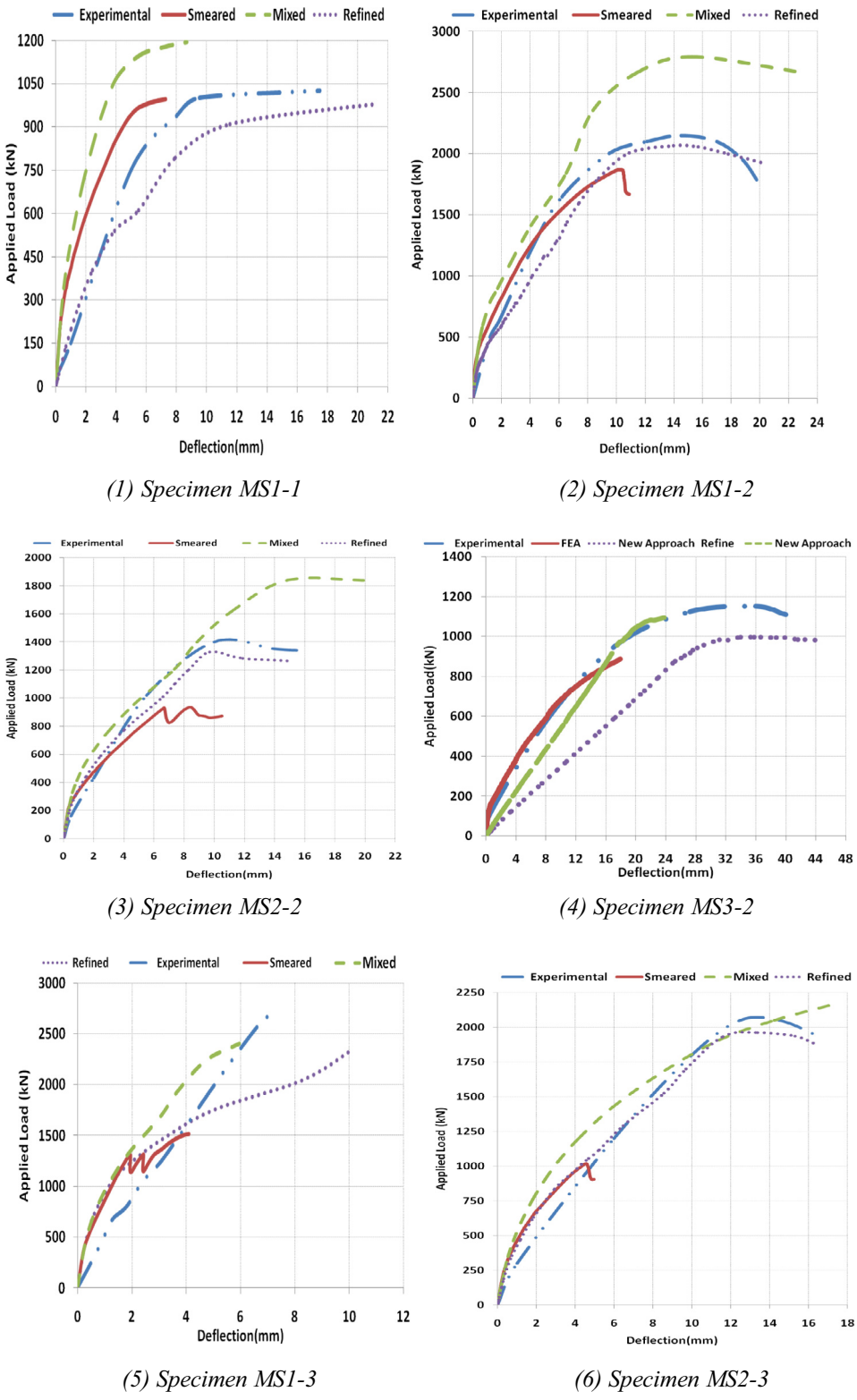

Fig. 9 Load versus mid-span deflection for beams with transverse reinforcement specimens.

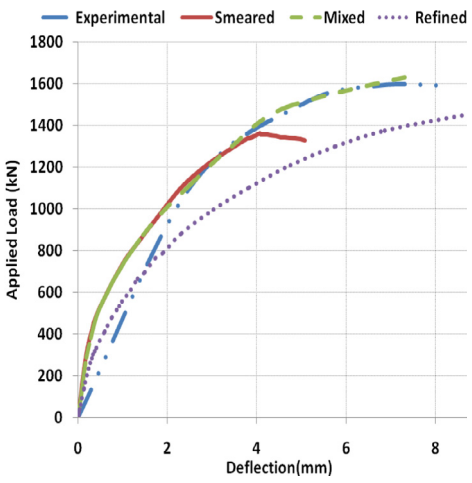

(7) Specimen NS1-4

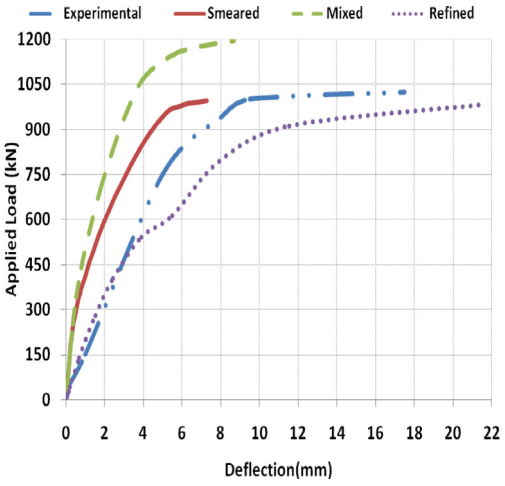

(8) Specimen NS2-4

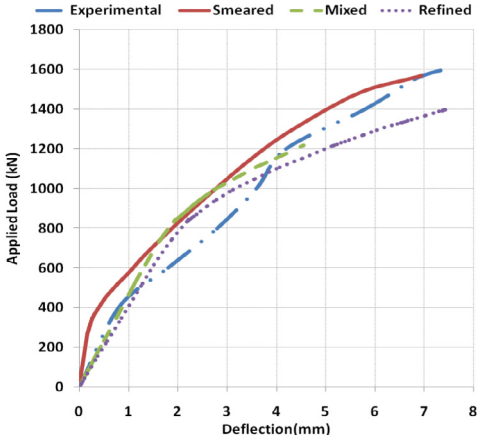

(9) Specimen MW1-2

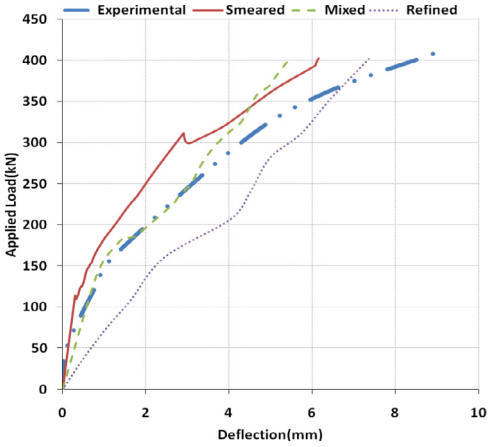

(10) Specimen MW3-2

Fig. 9 *(continued)*

Conclusions

1) The proposed mixed smeared/discrete cracking model approach shows better correlations with the experimental data.
2) Reinforced concrete beam initial modeled stiffness properties can be decreased by predicting the failure mechanism through modeling of the failure surfaces in the original intact reinforced concrete beam. One or more predicted failure surfaces may be used.
3) Beams with higher reinforcement ratio require more number of predicted surfaces due to higher stiffness caused by the additional reinforcement.
4) More slender beams require more number of discrete cracking surfaces with low inclination angles due to large shear spans which require more distribution of discrete cracking surfaces.

Conflict of interest

These authors declare no conflict of interest.

References

[1] S. Farooq, A. Rafeeqi, T. Ayub, Behavior of reinforced concrete beams detailed for shear in compliance with compressive force path method, NED University Journal of Research - Structural Mechanics 10 (2013) 13–14.
[2] A. Arabzadeh, R. Aghayari, A. Rahai, Investigation of experimental and analytical shear strength of reinforced concrete deep beams, Int. J. Civil Eng. 9 (2011) 2–5.
[3] J. Dedios, A. Lubell, Behavior of concrete deep beams with high strength reinforcement, University of Alberta, Structural Engineering Report 277 (2008) 39–162.
[4] P. Kmiecik, M. Kamiński, Modeling of reinforced concrete structures and composite structures with concrete strength degradation taken into consideration, Arch. Civil Mech. Eng. 11 (2011) 6–13.
[5] F.J. Vecchio, Analysis of shear-critical reinforced concrete beams, ACI Struct. J. 97-S12 (2000) 2–5.
[6] Vecchio, F. J., Non-linear Finite element analysis of reinforced concrete. ACI Special publication, Finite Element Analysis of Reinforced Concrete Structures 2002, SP-205:1–14.
[7] F. Vecchio, D. Lai, Crack shear slip in reinforced concrete elements, J. Adv. Concrete Technol. 3 (2004) 289–300.